CHALMERS
UNIVERSITY OF TECHNOLOGY

Durable Activated Carbon Electrodes with a Green Binder

Downloaded from: https://research.chalmers.se, 2025-12-04 16:33 UTC

Citation for the original published paper (version of record):
Rajendra Babu Kalai Arasi, A., Haque, M., Vyas, A. et al (2022). Durable Activated Carbon Electrodes with a Green Binder. Physica Status Solidi (B): Basic Research, 259(2). http://dx.doi.org/10.1002/pssb.202100311

N.B. When citing this work, cite the original published paper.

research.chalmers.se offers the possibility of retrieving research publications produced at Chalmers University of Technology. It covers all kind of research output: articles, dissertations, conference papers, reports etc. since 2004. research.chalmers.se is administrated and maintained by Chalmers Library

(article starts on next page)

physica status solidi b
www.pss-b.com

Durable Activated Carbon Electrodes with a Green Binder

Azega R. K., Mohammad Mazharul Haque, Agin Vyas, Pui Lam Tam, Anderson D. Smith, Per Lundgren, and Peter Enoksson*

Herein, the fabrication and electrochemical performance of thick (180–280 μm) activated carbon (AC) electrodes with carbonized lignin-derived carbon fiber (LCF) inclusions are reported. Efforts are taken in fabricating robust free-standing electrodes from an environmentally friendly binder, microfibrillated cellulose (MFC), considering the biologically hazardous nature of other commonly used binders like polytetrafluoroethylene (PTFE), n-methyl-2-pyrrolidone (NMP), and polyvinylidene fluoride (PVDF). Generally, electrodes composed of MFC binder are prone to cracking upon drying, especially with higher mass loadings, which leads to nonflexibility and poor device stability. The LCF inclusions into the AC electrode with MFC binders not only increase flexibility but also contribute to better conductivity in the electrodes. The LCFs act as an intermediate layer among AC particles and serve as conductive pathways, facilitating exposure of more active surfaces to the electrolyte. A thick electrode with high mass loading of 10 mg cm^{-2} is achieved. The results show that by incorporating 2 wt% LCF to the AC material, the best device with 5 mg cm^{-2} delivers a specific capacitance of 97 F g^{-1}, while the specific capacitance of the reference AC device without LCF is 85 F g^{-1}.

1. Introduction

Activated carbon (AC) is the predominant commercial choice of electrode material for charge storage in supercapacitors today. AC has an advantageous high surface area, and its mature manufacturing technology makes it a convenient commercially available low-cost material. Generally, environmentally unsafe fluorinated polymers have been used as binders to fabricate supercapacitors and battery electrodes to bind the AC particles together alongside conductive agents like carbon black (CB).[1] As alternatives, carboxymethyl cellulose (CMC), starch, casein, and natural polymers have been some of the green binder material choices.[2,3] In the interest of moving toward ecofriendly electrodes, a trial to use a cellulose-based binder, microfibrillated cellulose (MFC), is undertaken. The good binding property of MFC facilitates an increased packing density of the material, which is highly beneficial for the synthesis of thick electrodes. Utilizing such thick electrodes is a viable strategy to increase the stored charge per packaged device, as they contain more material compared with thin electrodes. However, the capacitive contribution from the deeper parts of the thick electrodes is insignificant if they are limited by the through-plane conductivity or inaccessible to the electrolyte ions in the system, which is typically the case. Therefore, the involvement of highly packed or mass-loaded electrodes risks the rate capability and specific power performance of the device. To resolve such issues, the incorporation of engineered structured materials such as quantum dots,[4,5] carbon nanomaterials,[6–8] MXenes,[9] and microspheres[10] into the electrode materials is a promising solution as they serve as good conductive pathways aiding through-plane conductivity of the electrodes with improved dynamics. For example, Gryglewicz et al. demonstrated a composite material containing ACs grafted with carbon nanofibers (CNFs) deposited by a chemical vapor deposition (CVD) process through the decomposition of propane with a 5% Ni catalyst. The composite material with shorter carbon fibers showed better electrical double layer capacitor (EDLC) performances explained by the presence of herringbone CNFs enacting as electronic bridges between AC particles facilitating better diffusion of ions.[11] Carbon nanotubes' inclusions in AC matrix provisions as channels for charge transport, improving site accessibility.[12] Polyacrylonitrile precursor-based conductive carbon fibers function as current collectors for depositing AC particles for flexible supercapacitors.[13]

Azega R. K., M. M. Haque, A. Vyas, P. Lundgren, P. Enoksson
Micro-Nano Systems Group
Electronics Materials and Systems
Department of Microtechnology and Nanoscience
Chalmers University of Technology
412 58 Gothenburg, Sweden
E-mail: azega@chalmers.se

A. D. Smith
Department of Electrical Engineering
Chalmers University of Technology
Hörsalvägen 7, 41296 Gothenburg, Sweden

P. L. Tam
Department of Industrial and Materials Science
Chalmers University of Technology
Rännvägen 2A, 412 96 Gothenburg, Sweden

P. Enoksson
Enoaviatech AB
112 26 Stockholm, Sweden

P. Enoksson
Smoltek AB
Kaserntorget 7, 411 18 Gothenburg, DS, Sweden

The ORCID identification number(s) for the author(s) of this article can be found under https://doi.org/10.1002/pssb.202100311.

© 2022 The Authors. physica status solidi (b) basic solid state physics published by Wiley-VCH GmbH. This is an open access article under the terms of the Creative Commons Attribution License, which permits use, distribution and reproduction in any medium, provided the original work is properly cited.

DOI: 10.1002/pssb.202100311

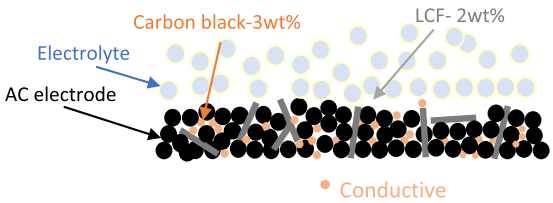

Figure 1. Schematic representation of the AC/LCF electrode depicting the fibers as reinforcements for the AC particles to be held together and its in-plane and through-plane conductive contribution in the AC matrix.

Likewise, lignin-based carbon fibers (LCFs) synthesized under optimized stabilization and carbonization conditions are well known for their higher graphitic nature contributing to higher electrical conductivity besides their function as a superior active material and current collector for the electrodes.[14] Apart from that, the fibers synthesized by the melt-spinning process have a high interfacial shear strength.[15]

Therefore, in this work, we have synthesized electrodes of different mass loadings by incorporating LCF in the commercially available AC material and characterized their initial electrochemical performance. The scope is to analyze the contributions of LCFs as a conductive agent (**Figure 1**) compared with the AC electrodes with only CB as the conductive agent.

2. Experimental Section

2.1. Materials

AC from the TCI chemicals supplier was used as the main component of electrode materials. The conductive agents, CB and LCF (carbonized at 1000 °C), were supplied by RISE in Sweden. MFC with 2.1% dry content was used as the electrode binder material.

2.2. Fabrication of AC/LCF Electrodes

The vacuum-dried samples of AC powder, 3 wt% CB, and 2 wt% LCF were mixed with 5 wt% MFC to prepare a suspension that was stirred overnight. The suspension with different mass loadings, 5, 7, and 10 mg cm^{-2}, was transferred to glass Petri dishes in the open air for a maximum of 2 days to prepare freestanding films. Afterward, the freestanding films were dried in the furnace for 4 h at 75 °C under vacuum to minimize the moisture. The reference electrodes without LCF were prepared in a similar procedure but with an increased CB amount of 5 wt%. Finally, the freestanding electrodes were punched out from the films with a circular disc cutter. The diameter of the individual electrodes was 8 mm.

Throughout this work, pure AC electrodes and LCFs that included AC electrodes were named AC-n and AC/LCF-n, respectively, where the n indicates the mass loadings, which were 5, 7, or 10 mg cm^{-2}. Their corresponding thicknesses were 180, 220, and 280 μm, respectively, with uncertainties lesser than ±5 μm.

2.3. Materials' Characterization

Scanning electron microscopy (SEM) LEO Ultra 55 was used to analyze the fiber morphology of the electrospun LCF. The secondary-electron detector was used to analyze the fiber surface in a high-vacuum mode of 3 kV, while the microscope operated at 1 kV accelerating voltage.

The conductivity measurements of LCFs were carried out with a Keithley 2400 conductivity analyzer. The resistivity, ρ, reciprocal of conductivity σ was calculated using the standard four-point probe formula

$$\sigma = \left[\frac{V}{I} \cdot \frac{w \cdot t}{s}\right]^{-1} \tag{1}$$

where V stands for the voltage difference, I for the current, w the fiber width, t for the fiber thickness, and s separation between the electrodes.

Surface composition and the chemical states of the elements of interests were studied by means of X-ray photoelectron spectroscopy (XPS). PHI 5000 VersaProbe III Scanning XPS Microprobe equipped with a monochromatic Al Kα X-ray source of photon energy 1486.6 eV was used, and the used beam size was set at 100 μm. For the insufficient sample conductivity, dual-charge compensation by an electron neutralizer and argon-ion gun was applied during the measurements. Surface composition was evaluated based on the survey scan with a wide scanning energy range between 0 and 1250 eV; the pass energy was at 280 eV and step size was at 1.0 eV. To analyze the chemical states of each element, high-resolution regional scans were conducted with the pass energy 26 eV and step size 0.1 eV. Prior to the qualitative analysis, the results from narrow scans were aligned with the adventitious carbon C 1s peak at 284.8 eV. The energy scale of the system, in contrast, was calibrated with reference to ISO 15 472:2010, in which the core levels of pure gold (Au $4f_{7/2}$), silver (Ag $3d_{5/2}$), and copper (Cu $2p_{3/2}$) were aligned at 83.96, 368.21, and 932.62 eV, respectively. Peak deconvolution was conducted using the MultiPak software. The spectra were first fit above the Shirley background, and the fit peaks were assigned at a specific energy peak position in the spectral envelope. Gaussian–Lorenztian function was used to fit the peak shape, and the full width at half maximum (FWHM) of the peak width was less than 2.0 eV in all the fitted curves. The contributions of each chemical state in a specific element were determined with reference to the area ratios of the fit peaks in the spectral envelope.

2.4. Electrochemical Measurements

The electrochemical performance was studied for a symmetrical supercapacitor device containing two similar electrodes assembled in a CR2025 coin cell, as shown in **Figure 2**. For their construction, the two identically mass-loaded electrodes were electrically isolated with a Whatman glass fiber membrane separator (10 mm in diameter). The assembled sandwich structure containing the aforementioned materials was soaked with 50 μL of 6 M KOH electrolyte before encapsulating the device.

Electrochemical measurements were carried out by cyclic voltammetry (CV), galvanostatic charge–discharge (GCD), cyclic charge–discharge (CCD), and electrochemical impedance spectroscopy (EIS) using a Gamry Reference 3000AE electrochemical workstation. The specific capacitance ($C_{s,CV}$ in F g^{-1}) was measured from CV data using Equation (2), as follows:

© 2022 The Authors. physica status solidi (b) basic solid state physics published by Wiley-VCH GmbH

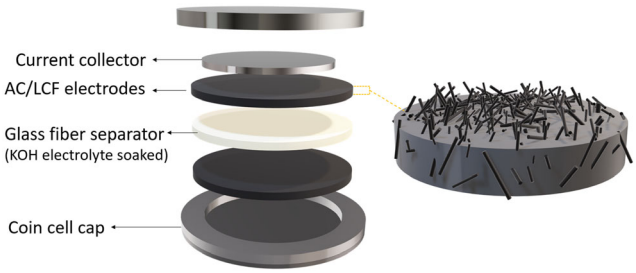

Figure 2. Schematic representation of the device construction with the prepared electrodes.[16]

$$C_{s,CV} = 4 \times 1000 \times \frac{\int_0^{2\cdot\Delta V/\nu_s} |i| dt}{2 \cdot m \cdot \Delta V} \quad (2)$$

where $I(A)$ is the current, ν is the scan rate, ΔV is the operating voltage window, and m is the mass of both the electrodes in the cell. The specific capacitances ($C_{s,GCD}$ in F g^{-1}) from GCD curves were calculated using Equation (3) as follows:[16]

$$C_{s,GCD} = 4 \times \frac{I_d \cdot t_d}{m \cdot V_d} \quad (3)$$

where I_d is the discharge current, t_d is the discharge time, and V_d is the voltage from the discharge curve excluding the internal resistance (IR) drop.

In addition, energy density (E in Wh kg^{-1}) and average power density (P_{avg} in W kg^{-1}) of the device are calculated from GCD curves, according to the following equations.[16]

$$C_d = \frac{C_{s,GCD}}{4} \quad (4)$$

$$E = \frac{1}{2} \times \frac{C_d \cdot {V_d}^2}{3.6} \quad (5)$$

$$P_{avg} = 3600 \times \frac{E}{t_d} \quad (6)$$

where the 3.6 and 3600 are unit time conversion factors. To calculate the specific device capacitance C_d, the $C_{s,GCD}$ values were divided by a factor of 4.

3. Results and Discussion

3.1. Material Characterization

The MFC-based electrodes are freestanding and not prone to breakage without stress. Under all mass loadings, the LCF alongside CB and MFC binder cooperated in holding the AC particles well, while the electrodes without LCFs were quite fragile during device assembly. **Figure 3**a shows the magnified SEM image of the AC electrode with large-sized AC particles ranging between 10 and 15 µm. The LCF fiber included in the AC matrix has a diameter of 13 µm and lengths ranging between 300 and 400 µm. The distribution of the fibers was observed to be uniform throughout the electrode even with the small LCF inclusion wt%. The low-magnification SEM image from a cracked middle cross section of AC/LCF-10 in Figure 3b shows the functionality of LCF as reinforcement in holding the AC particles together.

In addition, the LCF's measurements from the four-point probe show resistivity of 0.03 Ω cm, assuring their highly conductive nature that eventually facilitates good electronic conductivity to the AC particles in deeper layers, as demonstrated in Figure 1. Moreover, the observed unfilled voids around the AC electrode particle–LCF interface besides other voids additionally could aid in electrolyte impregnation as remarked for some commercial electrodes.[17] For further improvement of the electrode flexibility, the MFC binding could be complemented with strong elastomeric materials like styrene–butadiene–rubber (SBR).[18,19]

Figure 4a shows the survey-scan spectra from the XPS measurements of the AC and AC/LCF electrodes. Both samples show two distinct peaks. They correspond to carbon (C1s ≅ 284.8 eV) and oxygen (O1s ≅ 532.7 eV), respectively.

Results from XPS and XRD (see Figure S1, Supporting Information) show that LCF, as an additive, does not modify the surface composition of the AC electrode. However, in view of chemical state analyses, the contributions from carboxylic (COO^-), hydroxyl (–OH), and ketone (C=O) groups were altered. A slight increase in the carboxylic group and a significant increase in quinone/ketone groups are observed for the AC electrodes (Figure 4b). The presence of quinone/ketone groups usually contributes to an increased pseudocapacitance[20] that originates from the redox reaction by hydroquinone/quinone moieties in the system. The additional quinone groups for AC electrodes indicate the reduced availability of these redox functional groups by adding LCF inclusion to AC electrode. With corresponding conversion procedures, LCF–OH could be modified to form additional hydroquinones, which could potentially add to AC/LCF electrodes' pseudocapacitance.[21]

3.2. Electrochemical Performance

The CV curves of electrodes with mass loadings of 5 and 7 mg cm^{-2} at 20 mV s^{-1} scan rate, are shown in **Figure 5**a. The electrode's ability to store charge with 6 M KOH electrolyte was found effective in the electrochemical voltage window of 0–0.8 V. An EDLC-based reversible capacitive behavior is observed for both the electrodes as the CV curves exhibit a typical rectangular shape. The specific capacitance value for AC/LCF-5 is calculated to be 97 F g^{-1}, while for the AC-5, it is 85 F g^{-1}. However, with increasing mass loadings of 7 and 10 mg cm^{-2}, the capacitance values remain similar for both the AC and AC/LCF electrodes, especially at higher scan rates of 100 mV s^{-1} and above. The additional specific capacitance of the AC/LCF electrodes at lower scan rates suggests that the LCF promotes better ion penetration into the pores but only at a limited rate.

The GCD curves at a current density of 1 A g^{-1} are shown in Figure 5b. The curves are almost symmetrically triangular but have a small IR drop for all devices regardless of their electrodes. It is slightly larger for the electrodes with higher mass loading of 7 mg cm^{-2}, and it is higher by about 13 mV in AC electrodes compared with AC/LCF electrodes, indicating slightly lower IRs at 5 mg cm^{-2} mass loading. The AC electrodes with

© 2022 The Authors. physica status solidi (b) basic solid state physics published by Wiley-VCH GmbH

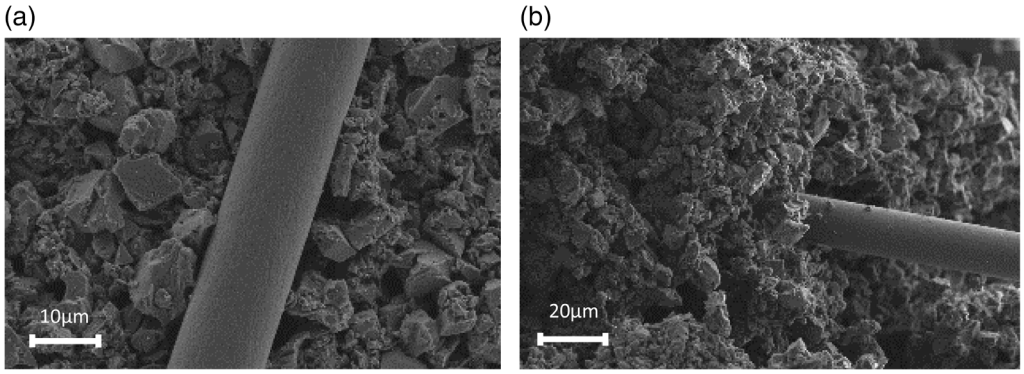

Figure 3. SEM images of a) AC/LCF electrodes fabricated with MFC as the binder and b) LCF reaching intermediary AC layers.

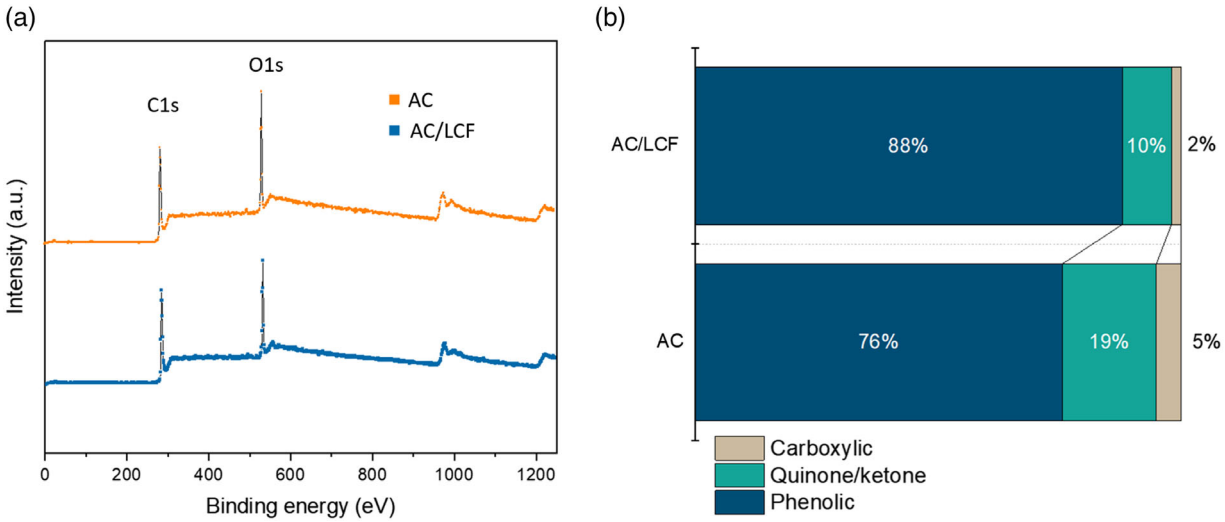

Figure 4. a) XPS broad-scan spectra of AC and AC/LCF samples. b) Distribution of predominant reactive and pseudocapacitive chemical states in the samples.

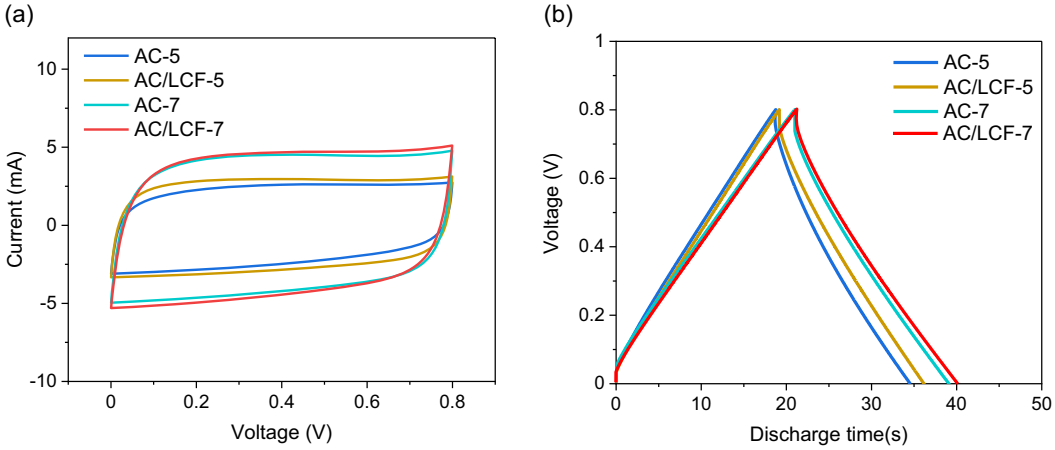

Figure 5. AC and AC/LCF electrode's (with mass loadings of 5 and 7 mg cm^{-2}) a) CV at 20 mV s^{-1} scan rate and b) GCD curve at 1 A g^{-1} current density.

CB-LCF and only CB as conductive agent delivered an energy density of 34 and 31 Wh kg^{-1}, respectively, at approximately the same power density of 71 kW kg^{-1}.

Figure 6 shows the EIS in the form of a Nyquist plot performed in the frequency range from 100 kHz to 10 mHz with an alternating current (ac) perturbation of 10 mV.

© 2022 The Authors. physica status solidi (b) basic solid state physics published by Wiley-VCH GmbH

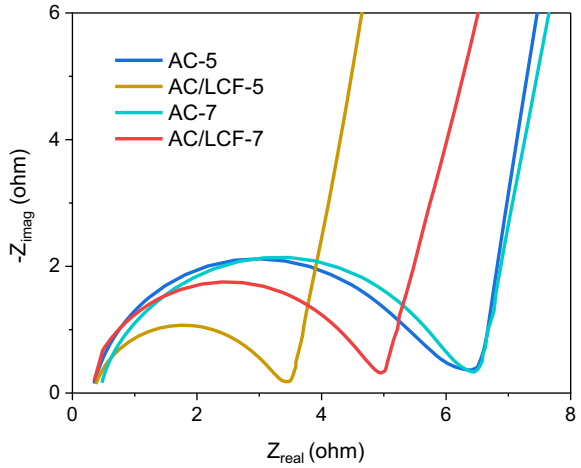

Figure 6. Nyquist plot for AC and AC/LCF electrodes at 5 and 7 mg cm^{-2} mass loadings (enlarged images of the high- and intermediate-frequency region).

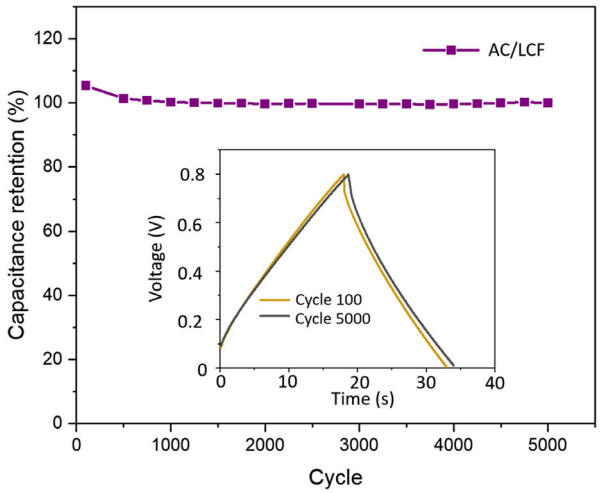

Figure 7. The specific capacitance of AC and AC/LCF electrodes at 5 mg cm^{-2} mass loading over 5000 cycles (inset: charge–discharge cycles of the same AC/LCF electrode during different cycling intervals).

The second intersection of the semicircle in the x-axis represents the charge transfer resistance or interfacial resistance that mostly originates from the electrode/electrolyte interface or electrode/current collector interface. However, as the first intersection representing electrolyte resistance is similar for all the devices, the resistances are confirmed to not originate from electrolyte wetting. As shown, the interfacial resistance is lower for the AC/LCF electrodes compared with pure ACs, which further confirms the contribution of LCF in the overall enhanced capacitance observed in CV and GCD measurements. However, with high mass loading of 10 mg cm^{-2}, the interfacial resistance increased for both electrodes, that is, the contributions from lesser LCF mass loadings for such thicker electrodes contributed to as much charge transfer resistance as AC electrodes devoid of added inclusion (Figure S2, Supporting Information). The increased charge transfer resistance is supposedly due to the limited space/volume available in the coin cell. The possibility to accommodate electrodes with only certain thickness affects the contact between electrode and stainless steel current collector. Cramping the cell with high pressure could create microfractures in thicker electrodes, decreasing the electrical conductivity contributions from LCF.

Additional modifications are necessary to truly utilize the useful features of LCF in the electrodes with a high mass loading. For instance, lowering the fiber diameter to a nanometer scale would potentially enhance the interaction between LCF and AC particles as a consequence of the larger available surface area.[11] As realized from the LCFs' SEM images, with a diameter of 13 μm, the interaction of all the AC particles around the LCF is very unlikely. Fiber diameters, lengths, and orientations are all interesting parameters to control and observe the impact for optimized electrode behavior, as are LCF surface modifications or functionalization. A net increase of the LCF content would, according to our XPS interpretation, increase the prevalence of surface functional groups in the electrode, which could be predicted to enhance the overall pseudocapacitive contribution.

A cycling stability test for 5000 cycles is shown in **Figure 7**. As seen, the AC/LCF electrodes show high capacitance retention of 98% with negligible performance deterioration after 1000 cycles. A very similar retention rate is observed for pure AC electrodes, and we thus see no reason to suspect a detrimental effect on the device's long-term stability from the LCF inclusions.

4. Conclusions and Future Work

A freestanding AC/LCF supercapacitor electrode is successfully fabricated using an MFC binder. The LCF serves both as a reinforcement agent in binding AC particles and as a conductive pathway in the AC matrix. The CV measurements indicate that the device containing AC/LCF-5 electrodes has a higher specific capacitance of 97 F g^{-1} compared with the device containing AC-5 electrodes with 85 F g^{-1}. EIS analysis confirms the less-resistive behavior of the AC/LCF electrodes up to 7 mg cm^{-2} mass loadings compared with pure AC electrodes. From the investigation with 2 wt% of LCF inclusions, the improved performances are distinctly superior for the electrodes with a mass loading of 5 mg cm^{-2}. For higher mass loadings (10 mg cm^{-2}), the performance is quite similar with and without LCF inclusions. With the further weight optimization and the reduction of the fiber dimensions along with control of their orientation in the AC matrix, the capacitive performance could be further improved in the thicker and highly mass-loaded electrodes. Thicker electrodes are essential for high-energy performances, and the faster charge transfer utilizing active material from all sites offers high power. Therefore, efficient compositing of highly conductive materials with AC can potentially contribute to the enhancement of the overall performances in existing commercially available supercapacitors. The understanding of synergy in compositing these materials requires more research.

© 2022 The Authors. physica status solidi (b) basic solid state physics published by Wiley-VCH GmbH

Supporting Information

Supporting Information is available from the Wiley Online Library or from the author.

Acknowledgements

The authors acknowledge funding from Sweden's Wallenberg Wood Science Centre (WWSC) under Project 4.1.4.

Conflict of Interest

The authors declare no conflict of interest.

Data Availability Statement

The data that support the findings of this study are available from the corresponding author upon reasonable request.

Keywords

activated carbon, carbon fibers, cellulose, energy storage, lignin supercapacitors

Received: June 30, 2021
Revised: December 20, 2021
Published online:

[1] B. Dyatkin, V. Presser, M. Heon, M. R. Lukatskaya, M. Beidaghi, Y. Gogotsi, *Chem. Sustain. Energy Mater.* **2013**, *6*, 2269.
[2] D. Bresser, D. Buchholz, A. Moretti, A. Varzi, S. Passerini, *Energy Environ. Sci.* **2018**, *11*, 3096.
[3] P. Ruschhaupt, A. Varzi, S. Passerini, *Energy Mater.* **2020**, *13*, 763.
[4] W. Tian, J. Zhu, Y. Dong, J. Zhao, J. Li, N. Guo, H. Lin, S. Zhang, D. Jia, *Carbon* **2020**, *161*, 89.
[5] Y. Qing, Y. Qian, H. Lin, L. Wang, A. Liu, Y. Cao, R. Sheng, G. Yong, C. Fan, S. Zhang, D. Jia, Z. Fan, *J. Mater. Chem. A* **2019**, *7*, 6021.
[6] F. Cheng, X. Yang, S. Zhang, W. Lu, *J. Power Sources* **2020**, *450*, 227678.
[7] M. Mahmudul Huq, C.-T. Hsieh, C.-Y. Ho, *Diamond Relat. Mater.* **2016**, *62*, 58.
[8] C. Portet, P. L. Taberna, P. Simon, E. Flahaut, *J. Power Sources* **2005**, *139*, 371.
[9] A. Vahid Mohammadi, J. Moncada, H. Chen, E. Kayali, J. Orangi, C. A. Carrero, M. Beidaghi, *J. Mater. Chem. A* **2018**, *6*, 22123.
[10] A.-Y. Lo, C.-C. Chang, Y.-W. Lai, P.-R. Chen, B.-C. Xu, *ACS Omega* **2020**, *5*, 11522.
[11] G. Gryglewicz, A. Sliwak, F. Beguin, *ChemSusChem* **2013**, *6*, 1516.
[12] Y. Zhou, P. Jin, Y. Zhou, Y. Zhu, *Sci. Rep.* **2018**, *8*, 9005.
[13] S. Zhai, W. Jiang, L. Wei, H. E. Karahan, Y. Yuan, A. Keong Ng, Y. Chen, *Mater. Horizon* **2015**, *2*, 598.
[14] W. E. Tenhaeff, O. Rios, K. More, M. A. McGuire, *Adv. Funct. Mater.* **2014**, *24*, 86.
[15] N. Meek, D. Penumadu, O. Hosseinaei, D. Harper, S. Young, T. Rials, *Compos. Sci. Technol.* **2016**, *137*, 60.
[16] M. Haque, I. Abdurrokhman, A. Idström, Q. Li, A. Rajaras, A. Martinelli, L. Evenäs, P. Lundgren, P. Enoksson, *Electrochim. Acta* **2022**, *403*, 139640.
[17] V. Obreja, *Int. Rev. Electr. Eng.* **2010**, *5*, 272.
[18] R. Wang, L. Feng, W. Yang, Y. Zhang, Y. Zhang, W. Bai, B. Liu, W. Zhang, Y. Chuan, Z. Zheng, H. Guan, *Nanoscale Res. Lett.* **2017**, *12*, 575.
[19] A. Kvasha, I. Urdampilleta, I. Meatza, M. Bengoechea, J. A. Blázquez, L. Yate, O. Miguel, H.-J. Grande, *Electrochim. Acta* **2016**, *215*, 238.
[20] G. Milczarek, *Electroanalysis* **2007**, *19*, 1411.
[21] B. Zhou, J. Li, W. Liu, H. Jiang, S. Li, L. Tan, L. Dong, L. She, Z. Wei, *Energy Mater.* **2020**, *13*, 2628.

© 2022 The Authors. physica status solidi (b) basic solid state physics published by Wiley-VCH GmbH